EFFECT OF SURFACE ROUGHNESS ON FRETTING WEAR BEHAVIOR OF CERAMIC COATINGS: A FINITE ELEMENT ANALYSIS

Yujie CHENG [1, 3], Mu YANG [2], Chong SU [1, *]

This study investigates the effects and mechanisms of surface roughness on the fretting wear process of ceramic coatings under full slip conditions. The uniform random perturbation is used to build ceramic coating surfaces of varying roughness and we design a finite element model. The fretting wore under an 80N and displacement amplitudes of 40μm and 60μm is simulated by accelerated simulation in a ball-on-flat contact model incorporating Archard's wear theory via UMESHMOTION. The results show that the wear depth and wear area increase with increasing surface roughness. At the displacement amplitude of 40μm, the maximum wear depth increases from 4.94μm at Ra = 0.6 to 7.71μm at Ra = 2.3 and becomes higher at 60μm where the depth increases as the displacement amplitude increases from 5.59μm to 8.92μm for the same roughness. The larger the displacement amount, the less uniform is the wear profile distribution. This reduces roughness for local wear variations. Surface roughness is the dominant factor in fretting. Under full slip condition due to large displacement amplitudes, the dominant wear mechanism switches from local stress concentration and spalling at microscopic asperity contacts to uniform material removal due to macroscopic sliding shear.

Keywords: Fretting wear; Ceramic coating; Surface roughness; Finite element simulation (FES)

1.Introduction

Fretting wear is a damage process involving small amplitude oscillatory motion between mated mechanical parts. In some, the bearings, blade-disk joints, electric contacts etc. can create fatigue cracks and enable them to propagate to failure [1–4].Since alumina is known to offer excellent wear resistance, ceramics such as alumina are widely applied to protect substrate surfaces [5-9].However, the surface finish of the ceramic coatings, often chosen by grinding, and roughness of the material, plays a critical role in their fretting wear [10-14].

[1*]School of Mechanical Engineering, Dalian Jiaotong University, Dalian 116028, China, e-mail: sc@djtu.edu.cn (Corresponding author)
[2]CRRC Dalian Locomotive & Rolling Stock Co. Ltd., Dalian 116028, China, e-mail: djtuym@163.com
[3]CRRC Zhuzhou Electric Locomotive Research Institute CO., LTD., Zhuzhou 412001, China, e-mail: 13321408061@163.com

Extensive research has been done by scholars in both experimental and simulation [15-18]. In experimental studies, Xu et al. [19] performed single-grit scratch tests for studying the effects of abrasive geometry and scratching parameters on material removal mechanism for ceramic for subsurface cracks initiation and propagation. Chen et al [20] investigated grinding and material removal mechanisms for three engineering ceramics at high speed with brazed diamond wheels based on the measurements of grinding forces and roughness. Kar et al. [21-23] analyzed the microstructure, phase composition, and residual stresses of ground plasma-sprayed ceramic coatings. They elucidated the relationship between coating structure and grinding performance, and found critical grind conditions for different thermally enhanced ceramic. Zhang et al., [24], discussed polishing performances of alumina ceramically with ultrasonic vibration assist, studying the effect of vibration parameters and abrasive properties on material smoothing performance and surface quality, and described a surface roughness prediction model. Choudhary et al. [25] analyzed application of various grinding fluids on the surface surfaces of alumina ceramics ground with electroplated diamond wheels, and discovered the lubrication process of additives on the ceramic.

In simulation studies, the finite element method (FEM) is widely used to simulate contact stresses and wear evolution. Archard wear model is used widely to predict wear volume. Even more accurate simulation is needed to simulate the surface landscape. Simulations based on the Weierstrass-Mandelbrot(W-M) fractal function describe surface in self-similar fashion but are not realistic enough to account for irregular morphologies of random brittle fracture in hard, brittle ceramics. It is not known how the specific ground shape of the ceramic coating, its roughness parameters and fretting wear behavior map into each other.

Accordingly, this study adopts the uniform random perturbation method to obtain surface with varying roughness. Together with Archard wear via the UMESHMOTION subroutine, a finite element model is proposed to explore the effect of surface roughness and displacement amplitude on fretting wearing behavior when full slip is utilized. This work provides theoretical support for increasing the surface quality of ceramic coating.

2.Fretting wear finite element model

2.1.Rough surface modeling

Complex rough surfaces are essential in tribology, wear, and contact mechanics and their coefficient of friction, contact properties, wear patterns and so on. Rough surface modeling is usually done via the W-M fractal function. It is continuous but non-differentiable, self-similar, and its fractal dimension can be varied and therefore appropriate for natural fractal surfaces. Despite the hardness and brittle nature of the ceramic coatings, there will always be random brittle

fracture when grinding. To better simulate these irregular fracture effects, we select a uniform random perturbation, for which the parameter R_a is linearly related to the maximum perturbations' amplitude. We use R_a, a statistical measure of microscopic undulations used to measure smoothness of surfaces, to obtain different values by controlling the maximum nodal offsets in 3 directions(Δx_{max},Δy_{max},Δz_{max}). The quantitative relation is determined by the following expression:

$$\Delta x_{max} = \pm R_a \times f_x \quad (1)$$

$$\Delta y_{max} = \pm R_a \times f_y \quad (2)$$

$$\Delta z_{max} = \pm R_a \times f_z \quad (3)$$

fx, fy, and *fz* define the linear relationship between R_a and maximum nodes. They are determined empirically, and their values depend on the surface of the coating. Roughness R_a is obtained by the formula:

$$R_a = \frac{1}{L}\int_0^L |y(x)|dx \quad (4)$$

Here, L represents the measured length; usually it is the surface length; $y(x)$ represents height deviation from the mean line at position x; therefore, the surface is shaped. R_a is the mean value of microscopic surface undulations: larger R_a is more surface undulated and more surface rough. Uniform random perturbation applies randomly a random offset to each surface node. The offset range is equal to R_a: larger and wider is the offset range. The area is rougher. Offsets for each node are given by a uniform distribution. The roughness Ra relationship is linear, and the perturbated range is $\pm R_a \times f$ (f is proportional). The offset for a node in each direction is given by:

$$\delta_x = random.uniform(-\Delta x_{max}, \Delta x_{max}) \quad (5)$$

$$\delta_y = random.uniform(-\Delta y_{max}, \Delta y_{max}) \quad (6)$$

$$\delta_z = random.uniform(-\Delta z_{max}, \Delta z_{max}) \quad (7)$$

Random.uniform(*a,b*) the random value uniformly distributed across the range (*a,b*). For example, if R_a =0.8, f = 1, the maximum nodal offset is: Δx_{max} =1×0.8=0.8. Instead of using other distributions, such as Gaussian, the uniform distribution guarantees that every offset within the range will be equally likely to be generated for each node. The main advantage of this is its simplicity and computational simplicity. Generating uniformly distributed random numbers is a cheaper way to obtain random numbers than sampling from other distributions (such as Gaussian). The perturbation range can be increased with the input roughness R_a value in order to simulate different roughness topographies. A Python script was developed to implement this method by randomly perturbing nodes in the meshed region in order producing surfaces with the following roughness values (For details of this script section, see Appendix 1): R_a = 0.6, 1.3, 1.8, and 2.3. After the node is generated, the coordinates were extracted to reconstruct the corresponding surface topography as shown in Fig. 1.

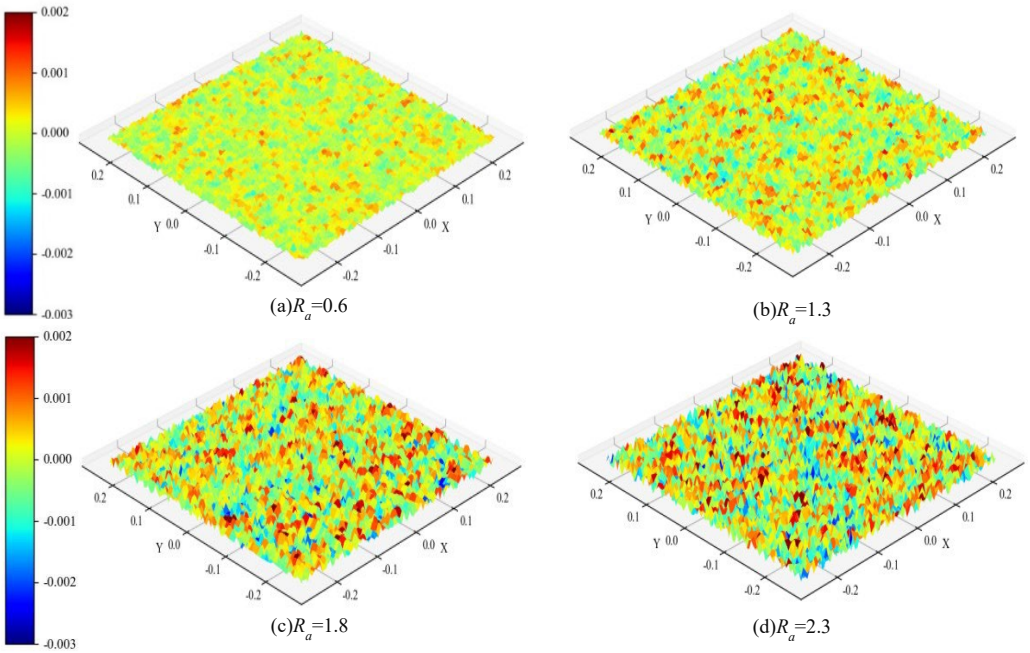

Fig. 1. Schematic diagram of surfaces with different roughness

In this script, you need to input the node set name, minimum displacement (Δx_{min}, Δy_{min}, Δz_{min}) and maximum displacement (Δx_{max}, Δy_{max}, Δz_{max}). Using these inputs, the script generates random node perturbations to simulate surfaces with varying roughness. Beyond its theoretical merits, the method demonstrates considerable practical utility in engineering applications. Its efficiency and flexibility make it particularly well-suited for simulating surface roughness in large-scale models [26].

2.2.Numerical Model Development

A sphere-on-flat contact model was developed. The upper specimen is an ISO K20 carbide ball, and the lower specimen is a 45steel plate coated with an alumina layer. Both specimens were geometrically simplified to reduce computational cost and mesh density. As shown in Figure 2(a), the lower specimen dimensions are 4mm×4mm×3mm. A mesh fitting study for accuracy was done. A coarse mesh (element size, 5μm) was applied only to the 0.5mm×0.5mm contact region of the lower specimen, and a coarser mesh was used elsewhere.

The bottom of the flat specimen, shown in Fig 2(b) is a cylinder with a spherical cap of 10mm diameter, a base radius of 0.20mm, and height of 0.25mm. Due to its hardness, the upper specimen was modeled as an analytic rigid body. The penalty function approach was used to model the contact interaction. The final set is shown in Figure 2(c).

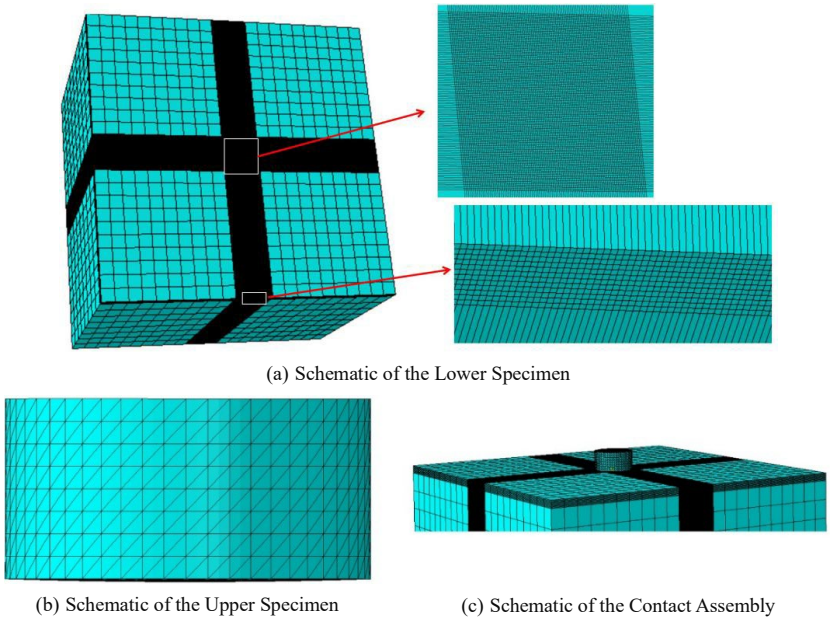

(a) Schematic of the Lower Specimen

(b) Schematic of the Upper Specimen

(c) Schematic of the Contact Assembly

Fig. 2. Schematic diagram of the finite element model of the upper and lower specimens

The bottom has been fixed in all directions. 80N contact pressure was applied to the bottom specimen and periodic displacement of different amplitude in *X*-direction to simulate fretting. Our initial tests showed that the coated surface had only partial slip with small displacement. With increasing amplitude, the behavior gradually changed to gross slip without a mixed slip regime. Since fretting wear involves more complex mechanisms in gross slip, we consider the fretting response in this case. Based on our preliminary fretting map, gross slip occurs with displacement amplitudes of 40μm and 60μm and cyclic displacements of 40μm and 60μm are applied in *X*. We applied three steps, Step 1 and Step 3 for applying and removing the normal load and Step 2 (main analysis) for applying the cyclic displacement to simulate the fretting response.

3.Fretting wear model

3.1.Archard wear model

Selecting a suitable wear model is important to allow accurate and reliable fretting wears simulation. Common models are Archard and energy-based models. Archard model is the one to use for low load, low-speed sliding problems, assuming constant friction coefficient and computing wear from normal load, sliding distance, and wear coefficient to simulate tremor [27–31]. The wear volume V is proportional to the normal (and sliding distance) load as reflected in:

$$V = k \cdot \frac{F \cdot d}{A \cdot H} \tag{8}$$

Here, k is wear coefficient, F is normal force, d is sliding distance, H is material hardness, and A is contact area. This means that the wear depth depends on the contact pressure and sliding distance and inversely on the hardness, which gives a theory for the wear prediction.

For minimizing the wear accumulation over time, we could build our model in the integral form for time. Therefore, the wear volume $V(t)$ for the dynamic case is:

$$V(t) = k \cdot \int_0^t \frac{F(\tau)\cdot v(\tau)}{H} d\tau \tag{9}$$

Here, $F(\tau)$ and $v(\tau)$ are instantaneous normal force and sliding velocity at time τ, respectively, H is material hardness, and k is wear coefficient. This form estimates wear accumulation during time, with dynamic loading and sliding speed. This can provide a model for estimating the wear during time when normal force/sliding velocity change.

In the case of complex contact, it could also use the Archard model to predict the wear distribution along the contact area by considering the variation of contact and sliding distances in space. With a local variation in the pressure and sliding distance and hardness, this can be used in the same form as the Archard model. For high load and large speed or time-varying friction coefficients, the Archard model might be employed to obtain the estimate of wear:

$$V(t) = \int_0^t \int_A k(x) \cdot \frac{F(x,\tau)\cdot v(x,\tau)}{H(x)} dA d\tau \tag{10}$$

Here, $F(x,\tau)$ and $v(x,\tau)$ are instantaneous normal force and sliding velocity, respectively, $H(x)$ is material hardness, and $k(x)$ is wear coefficient, all at position x and time τ. A is contact area and dA is an infinitesimal area element. This formulation could be used for modelling the wear in non-uniform contact conditions. In particular, for high loads and large speeds or time-varying friction coefficients, it may need to combine the Archard model to obtain accurate prediction.

In this study, wear depth is a measure of material removal and we chose the Archard model to calculate the wear. It was implemented as the UMESHMOTION subroutine to simulate fretting wear. The algorithm automatically called each step in order to estimate shear friction force and relative slip distance at every contact area node, providing information needed for calculating the wear profile. As an example, the local wear depth could be updated at every step for the real contact conditions to better model the evolution of the worn profile.

3.2.Accelerated computing

Fretting wear involves tens to hundreds of thousands of cycles. Doing the same for every period of wear would cost very much and cause heavy mesh distortion. In order to address this problem we proceed with a more accelerated simulation scheme. The wear profile change only after the onset of the ΔN fretting

cycles. All blocks of ΔN physical cycles are averaged together, taking one new step. During one move the UMESHMOTION subroutine accumulates the wear depth of ΔN cycles given the current contact state and updates the nodal coordinates once again. The formulation is:

$$h(x) = \Delta N \sum_q K_{eq}(x) d_s(x) \tag{11}$$

Here, $h(x)$ is the wear depth, ΔN is the number of cycles per increment, $Keq(x)$ is a friction-related coefficient, and $ds(x)$ is a damage-related variable. It accumulates wear over ΔN fretting cycles.

With this methodology, we only consider 12000 ΔN fretting cycles with only 12 increments (with ΔN=1000). We maintain the accuracy but very fast computations. By drastically reducing the number of moves without compromising the physical manifestation of the wear accumulation and by reducing the distortion of the meshes, the method offers considerable performance gains and enables us to perform finite element analysis of large-scale ΔN fretting cycles, which can be performed by means of nodal updates.

3.3.Node update

In FE simulations, updating the fretting wear profile relies on nodal updates. Wear entails continuous surface change, simulated in FE analysis by displacing mesh nodes. This process dynamically adjusts the mesh to reflect profile evolution during fretting cycles. We implemented the UMESSHMOTIONS subroutines in FORTRAN to compute nodal displacements and contact stresses during the fretting process. The Archard model calculates the wear depth, which will be used to update the nodes and the surface profile. This update induces no stress or strain. This is suitable for fretting wear simulations. However, over-placement of the nodal can cause very severe mesh distortion that can cause convergence. We applied ABAQUS ALE adaptive meshing to this model, shown in Figure 3.

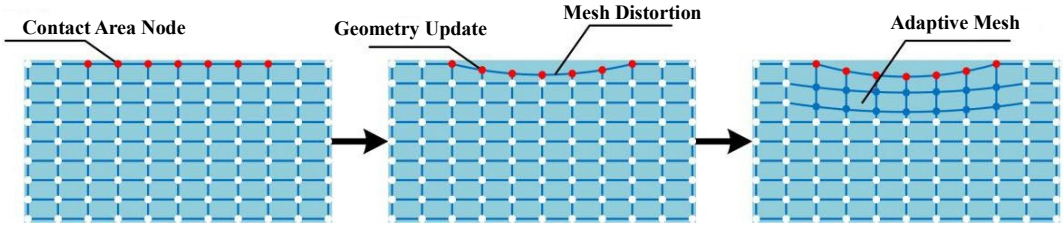

Fig. 3. Adaptive Mesh Refinement (AMR)

ALE adaptive meshing method, which is based on Lagrangian and Eulerian. The adaptive mesh rezoning is possible to keep mesh quality during large deformations to avoid distortion, provide computational stability, accuracy and time to get the final result. At each step, UMESHMOTION calls the Archard wear formula to compute wear of that step and is return to ABAQUS main solver for the final results. Therefore, an integrated simulation framework is developed based on

UMESHMOTION subroutine (simulation using the Archard wear model and updating nodes) and ALE (simulating the mesh quality), allowing efficient and stable simulation of the surface topography of fretting wear. The computed process and workflow are presented in the flowchart of Figure 4.

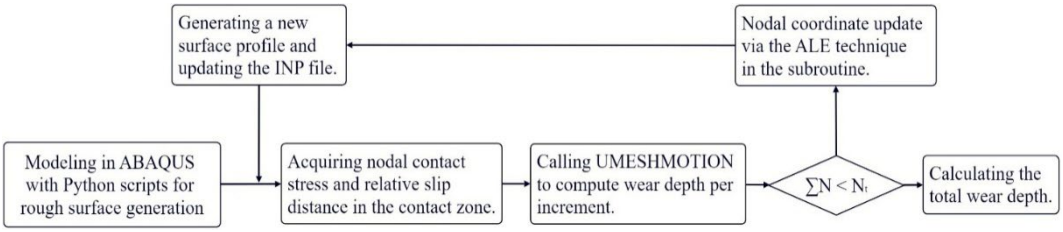

Fig.4. Flow chart of finite element simulation of fretting wear

4.Simulation results and analysis

Figure 5 presents the wear in normal load 80N and displacement amplitude 40μm for 4 different surface roughness levels. The worn surfaces had circular pits, indicating that the same operation was performed in full slip. The maximum value of the wear depth was 4.94μm at R_a=0.6. It expanded to 6.81μm at R_a=1.3 and increased to 7.39μm at the R_a=1.8, and continued to increase wear area. For the highest roughness at R_a=2.3, the increasing value of wear depth and area was smallest, at the highest value of 7.71μm.

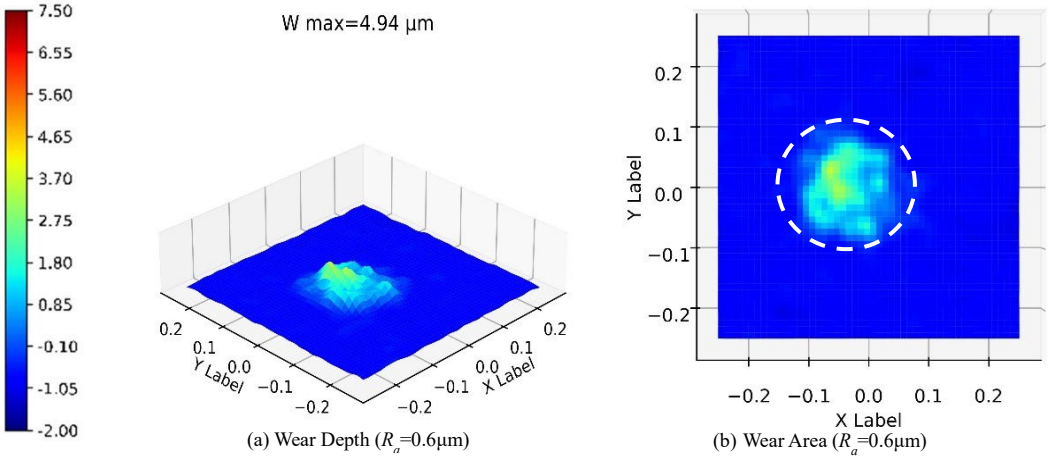

(a) Wear Depth (R_a=0.6μm) (b) Wear Area (R_a=0.6μm)

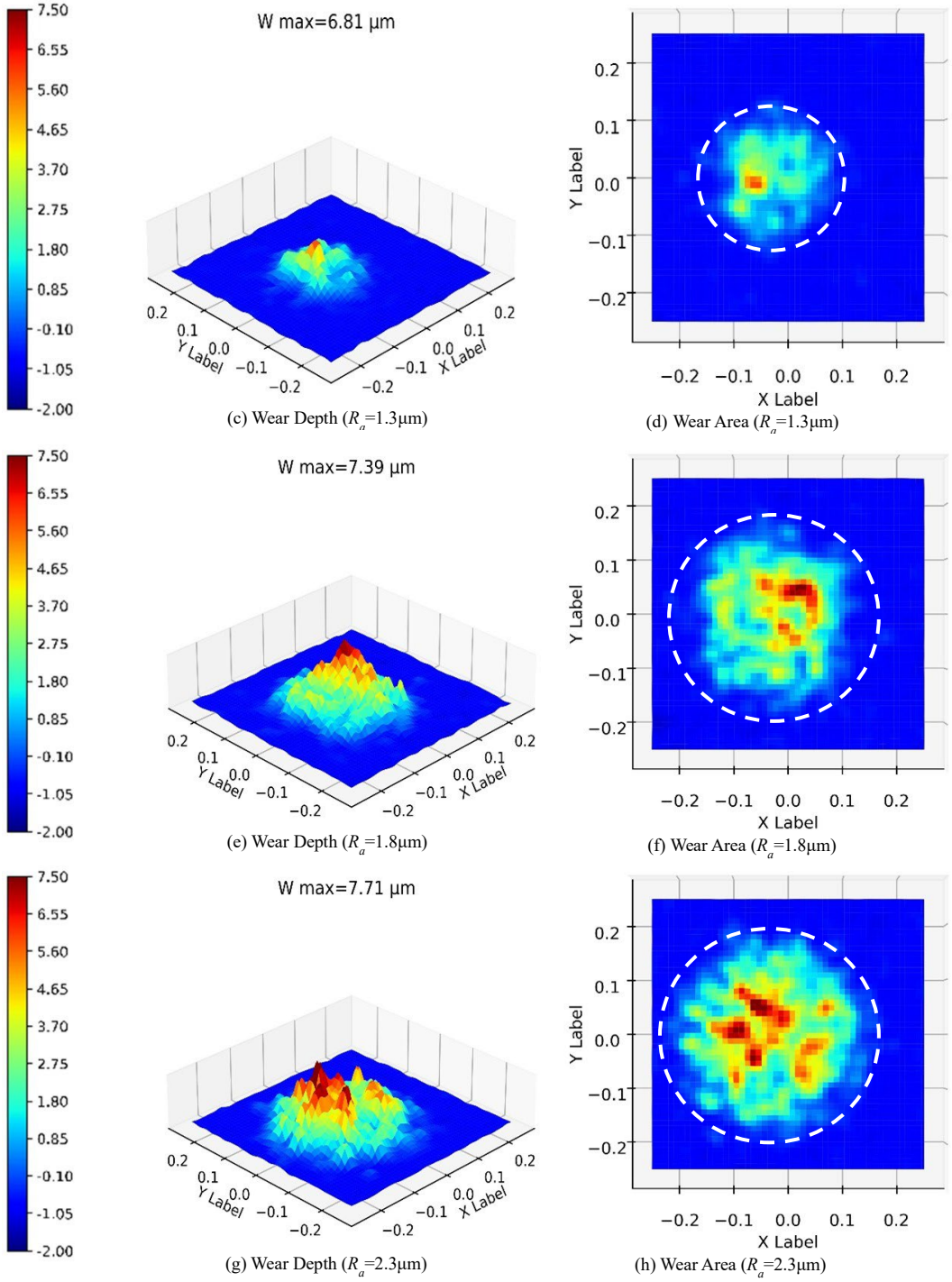

(c) Wear Depth (R_a=1.3μm) (d) Wear Area (R_a=1.3μm)

(e) Wear Depth (R_a=1.8μm) (f) Wear Area (R_a=1.8μm)

(g) Wear Depth (R_a=2.3μm) (h) Wear Area (R_a=2.3μm)

Fig. 5. Finite element simulation results of surfaces with different roughness at 40μm displacement amplitude

Surface roughness results in random asperities on the ceramic coating, where friction pair contact at the discrete asperity rather than as a flat surface. At large displacement amplitudes and large asperities weaken adhesion, allowing sliding and worse wear. Wear depth and the area increase with surface roughness.

Figure 6 presents the maximum values of the maximum value for 4 roughness with increasing displacement amplitude. The fretting wear increased significantly for all roughness values: it increased to 5.59μm at R_a=0.6, to 7.61μm at R_a=1.3 (with larger wear area), and continued of increasing 8.04μm at R_a=1.8 (with greater area growth). At the maximum R_a=2.3 wear depth added and increase but slow growth. Maximum value of 8.92μm. As in 40μm, the average wear depth increases and increases with roughness. The wear area is less sensitive to the influence of the area expansion of the roughness, while at 60μm, it is clear that under larger displacements, the area impact with the increasing surface roughs has a lower influence on the overall wear area increase.

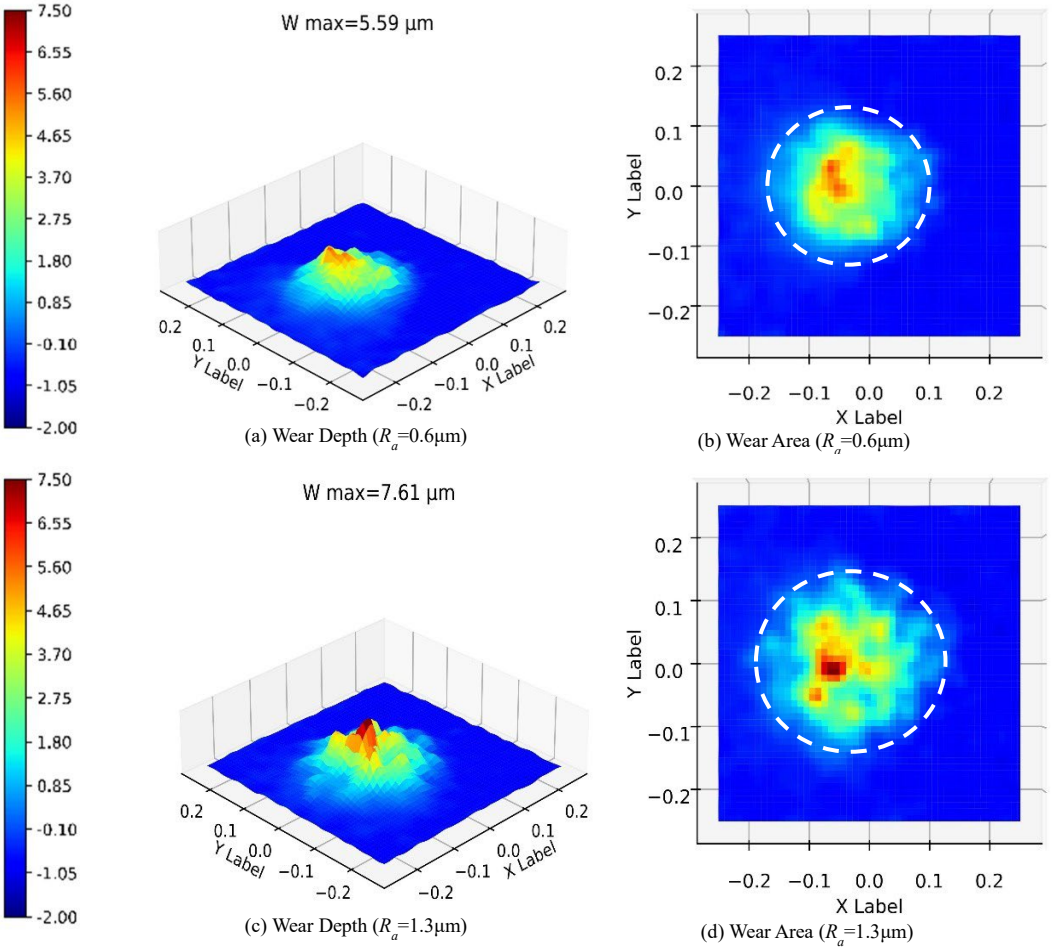

(a) Wear Depth (R_a=0.6μm)

(b) Wear Area (R_a=0.6μm)

(c) Wear Depth (R_a=1.3μm)

(d) Wear Area (R_a=1.3μm)

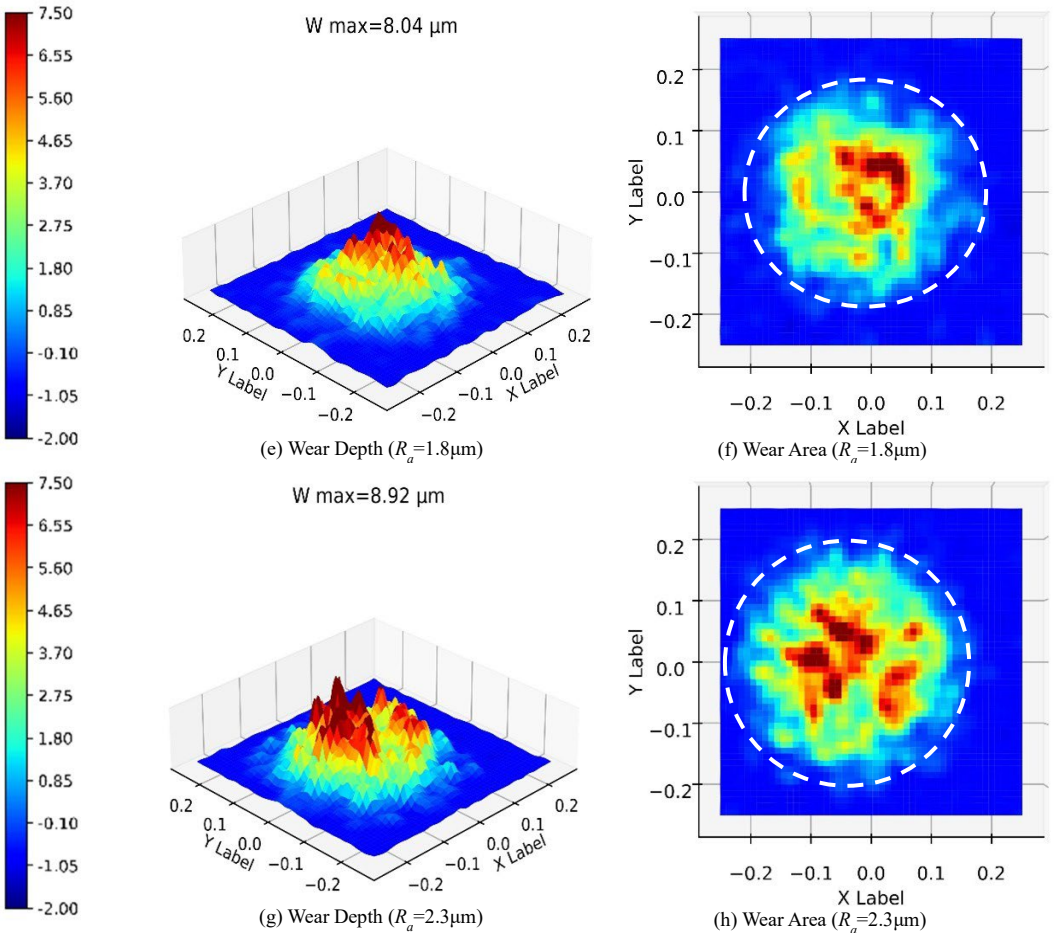

Fig. 6. Finite element simulation results of surfaces with different roughness at 60μm displacement amplitude

The relative stability of fretting wear with respect to surface roughness and displacement amplitudes indicates that surface roughness is dominant. The wear depth and area increase with surface roughness. For larger amplitudes, however, the uniformity of wear becomes more prominent. This is because at larger amplitude, sliding is more complete and when the asperities are sliding, the relative motion of the asperities becomes more constant.

This reduces the local stress concentration caused by the surface peaks and moves from local to more distributed wear. Moreover, as the sliding distance increases with the larger amplifications, the load transfer between contacting surfaces shifts from local or global. In this regime, the wear is dominated by the roughness more than individual asperity, leading to more uniformity.

In the same manner, material removed in the full-slip regime is picked up by macroscopic shear rather than microscopic spallation. The effect of roughness in wear morphology is smaller. While larger altitudinally, larger roughness still results in larger wear volumes, indicating that the initial surface topography is responsible for the main role of fretting wear.

5.Conclusions

This study proposes a finite element framework with uniformly randomized surface geometry to explain the fretting wear of ceramic coatings in gross slip. The relationship between surface geometry and motions was analyzed which resulted in theoretically and practically important results:

(1) Surface roughness regulates fretting wearing severity through contact stress distribution. There is positive correlation between R_a value and wear depth and area across 40μm and 60μm displacement amplitudes. The role of the underlying mechanism is due to stress concentrations caused by stochastic asperities, which lead to localized material removal.

(2) Displacement amplitude leads to uniformity of wear. The increasing displacement amplitude increases overall wear and alters the underlying wear mechanism. For a small amplitude (40μm), the wear morphology is dominated by local effects of surface asperity. For large amplitude (60μm), sufficient sliding leads to a more uniform wear, implying mechanistic transition from asperities-dominated localized spalling to macro-scale sliding-induced shear, hence the effect of surface roughness on wear distribution becomes less important.

(3) This study provides and validate a suitable simulation framework with three parts: surface generation by the uniform random perturbation method, wear simulation with the Archard model and mesh management with ALE adaptive meshing. Our framework enables accurate prediction of the fretting wear of the ceramic coating at all surface roughness levels, and provides a solid theoretical framework for optimizing the wear resistance of the surface finishing technique.

Acknowledgments

We would like to thank the project research partners and funding support units. This work was supported by the National Key R&D Program of China (2020YFB2007804) and Scientific Research Project of Liaoning Provincial Department of Education (JYTMS20230005)

REFERENCES

[1] *T. Zhang, K. Guo, J. Li, H. Yuan,* Experimental and computational investigations on fretting fatigue crack growth in dovetail joints, AIAA Journal, 60(8), 4893-4905, 2022.

[2] *J M. Dobromirski,* Variables of Fretting Process - Are There 50 of Them, Standardization of Fretting Fatigue Methods and Equipment, (1159), 60-66, 1992.

[3] *M. Zhu, Z. Zhou,* On the mechanisms of various fretting wear modes, Tribology International, 44(11):1378-1388, 2011.

[4] *P. Rycerz, A. Olver, A. Kadiric,* Propagation of surface initiated rolling contact fatigue cracks in bearing steel, International Journal of Fatigue, 97, 29-38, 2017.

[5] *Z. Bu, X. Zhao, X. Guo,* Electromotor bearing protection measures and research status of Al2O3 ceramic coating, Surface Technology, 50(5), 51-59, 2021.

[6] *C. Du, H. Xie, J. Liu, B. Lei, R. Zhang,* Improvement of Ti3SiC2/SiC composite ceramic friction and wear behavior by mechanical-friction oxidation synergism in a wide temperature domain of SiC, Wear, 572, 205984, 2025.

[7] *Y. Zhai, D. Gao, W. Chen,* Research Status of Tribological Behavior of Ceramic Materials in Harsh Environment, Chin. Ceram, 56(12), 1-9, 2020.

[8] *J. Zhang, C. Zhang, S. Zhang, W. Zhang,* Sliding friction and wear of B4C ceramics sintered with Al2O3/Y2O3, Journal of the European Ceramic Society, 44(13), 7556-7565, 2024.

[9] *BW. Luo, ZW. Wang, XB. Wu, CP. Wang,* Friction and wear behavior of paired pairs of ceramics and metal in high-pressure pump of seawater desalination, Strength of Materials, 53(5), 797-803, 2021.

[10] *Y. Feng, Q. Tan, H. Sun, Z. Zhang, X. Han, J. Peng, M. Zhu,* Investigation of the Fretting Friction and Wear Characteristics of G20Mn5QT Cast Steel Laser Cladding 316L Layer, TRIBOLOGY, 45(9), 1257-1270, 2024.

[11] *S. Atkinson,* Federal-Mogul Powertrain develops high-performance polymeric bearing coating for heavy-duty applications, Sealing Technology, 2019(1):7-7, 2019.

[12] *T H. Zhang, H. Yong,* Micro/nanomechanical and tribological properties of thin diamond-like carbon coatings, Chinese Journal of Aeronautics, 16(1): 47-51, 2003.

[13] *Z. Yuan, Z. Jiang, Z. Zhou, H. Wang, J. Li, Z. Cai, Z. Piao,* Effect of surface roughness on friction and wear behavior of GCr15 bearing steel under different loads, Surface Science and Technology, 2(1), 28, 2024.

[14] *W. Wei, Y. Su, H. Fan, H. Liang, J. Song, Y. Zhang, L. Hu,* Fretting Friction and Wear Characteristics and Damage Behaviors of Si3N4 Ceramic Balls Sliding against Bearing Steel, Tribology, 42(1), 113-122, 2021.

[15] *Z. Cao, L. Cui, S. Luo, H. Su, Z. Pang, W. Zhao, L. Zhang, W. He, X. Liang,* Superior fretting wear resistance of titanium alloys from stable gradient nanostructures induced by laser shock peening, International Journal of Plasticity, 188, 104293, 2025.

[16] *M. Odfalk, O. Vingsbo,* Influence of normal force and frequency in fretting©, Tribology transactions, 33(4): 604-610, 1990.

[17] *L. Xin,* Fretting wear behavior and damage mechanism of nuclear grade Inconel 690TT alloy, PhD Thesis, 2018.

[18] *B. Dang, X. L. Meng, D. Chen, K. Yang, T. Tian, D. B. Wei, P. Z. Zhang,* Mechanical, fretting wear and tribocorrosion properties of CrxN coatings on Zr-4 alloy prepared by double glow plasma alloying technology, Applied Surface Science, 692, 162683, 2025.

[19] *H H K. Xu, S. Jahanmir,* Microfracture and material removal in scratching of alumina, Journal of Materials Science, 30(9): 2235-2247, 1995.

[20] *J. Chen, J. Shen, H. Huang, X. Xu,* Grinding characteristics in high speed grinding of engineering ceramics with brazed diamond wheels, Journal of Materials Processing Technology, 210(6-7), 899-906, 2010.
[21] *S. Kar, P P. Bandyopadhyay, S. Paul,* Precision superabrasive grinding of plasma sprayed ceramic coatings, Ceramics International, 42(16): 19302-19319, 2016.
[22] *S. Kar, S. Kumar, P.P. Bandyopadhyay, S. Paul,* Grinding of hard and brittle ceramic coatings: Force analysis, Journal of the European Ceramic Society, 40(4): 1453-1461, 2020.
[23] *S. Kar, S. Paul, P.P. Bandyopadhyay,* Processing and characterisation of plasma sprayed oxides: Microstructure, phases and residual stress, Surface and Coatings Technology, 304: 364–374, 2016.
[24] *C. Zhang, Y. Liang, Z. Cui, F. Meng, J. Zhao, T. Yu,* Study on the effect of ultrasonic vibration-assisted polishing on the surface properties of alumina ceramic, Ceramics International, 48(15): 21389-21406,2022.
[25] *A. Choudhary, A. Naskar, S. Paul,* An investigation on application of nano-fluids in high speed grinding of sintered alumina, Journal of Manufacturing Processes, 35: 624-633, 2018.
[26] *Q. Zhou, J. Wang, Q. Wan, F. Jin, W. Yang, Q. Miao, Z. Wang,* Numerical analysis of the influence of distributed inhomogeneities on tangential fretting, Proceedings of the Institution of Mechanical Engineers, Part J: Journal of Engineering Tribology, 231(10), 1350-1370, 2017.
[27] *E. Muratović, N. Pervan, A. Muminović, M. Delić,* A Contact Mechanics Model for Surface Wear Prediction of Parallel-Axis Polymer Gears, Polymers, 16(20), 2858, 2024.\
[28] *TC. Huang, CY. Lin, KC. Liao,* Experimental and numerical investigations of the wear behavior and sealing performance of PTFE rotary lip seals based on the elasto-hydrodynamic analysis with considerations of the asperity contact, Tribology International, 187: 108747, 2023.
[29] *Y. Kim, J. Suh, B. Lee, Y. Chun, K. Park, Y. Yu,* Quasi-static sliding wear analysis of 3D rough surface considering changes in the point of contact, Applied Sciences, 12(23), 12465, 2022.
[30] *C. Wei, C. He, H. Tan, Y. Su, G. Chen, Y. Sun, C. Ren,* A predictive model for tool wear behavior during ultra-precision lapping, The International Journal of Advanced Manufacturing Technology, 136(2), 875-895, 2025.
[31] *JC. Martínez-Londoño, J. Martínez-Trinidad, A. Hernández-Fernández, RA. García-León,* Finite element analysis on AISI 316L stainless steel exposed to ball-on-flat dry sliding wear test, Transactions of the Indian Institute of Metals, 76(1), 97-106, 2023.

Appendix 1

```
set_name, xx, yy, zz, xx1, yy1, zz1 = getInputs
session. journalOptions. setValues(replayGeometry=INDEX,recoverGeometry=INDEX)
p = mdb.models['Model-1']. parts ['Part-1']
pp = mdb.models['Model-1']. parts['Part-1']. sets[set_name]. nodes
num_node = len(pp)                          aa = list(pp)
list1= []                                    for i in range(num_node):
list1.append(aa[i]. label)                   n = p.nodes
list2 = []                                  for j in range(num_node):
list2.append(n[int(list1[j])-1:int(list1[j])])
for nodes in list2:
p. editNode(nodes=nodes, offset1=random.uniform(-float(xx), float(xx1)),
offset2=random.uniform(-float(yy), float(yy1)),
offset3=random.uniform(-float(zz), float(zz1)))
print('done')
```